Band structure and optical properties of CuBr: new photoemission results

1993 J. Phys.: Condens. Matter 5 3827

(http://iopscience.iop.org/0953-8984/5/23/009)

J. Phys.: Condens. Matter 5 (1993) 3827–3836. Printed in the UK

Band structure and optical properties of CuBr: new photoemission results

R Matzdorf, J Skonieczny†, J Westhof, H Engelhard and A Goldmann
Fachbereich Physik, Universität Kassel, Heinrich-Plett-Strasse 40, D-3500 Kassel, Federal Republic of Germany

Received 21 September 1992, in final form 12 March 1993

Abstract. We have measured angle-resolved ultraviolet photoemission spectra from epitaxially grown thin films of CuBr with (111) orientation. Their analysis allows the determination of an experimental valence band dispersion very near the Γ-L-direction of the bulk Brillouin zone. These results show fair agreement with a KKR band structure calculation performed by Overhof. Our results, combined with earlier results obtained by 'constant-initial-state' photoelectron spectroscopy, are in agreement with all available optical data to within typically ±0.1 eV.

1. Introduction

The electronic properties of the noble metal halides are essentially determined by the energy positions and hybridization of the noble metal d orbitals, and the p orbitals of the halides [1]. This is in contrast to the isoelectronic III–V and II–VI compounds, where in general the d^{10} shells form deep core levels with virtually no energy dispersion. Thus the noble metal halides are interesting and sufficiently simple model substances to study hybridized p–d bonds.

Like most III–V and II–VI compounds, the copper halides (I–VII) are tetrahedrally coordinated semiconductors which crystallize in the zincblende lattice. However, while the usual bond in the zincblende structure is derived from an sp^3–sp^3 electronic configuration, the copper halide valence bands are formed by an sp^3–sd^3 configuration. The resulting p–d hybridization significantly changes the physical properties of the copper halides compared with the other members of the group IV, III–V and II–VI isomorphic series. For example, in CuCl the spin–orbit splitting of the edge exciton is reversed from that of the 'normal' zincblende materials [1]. Also the volume dependence of the spin–orbit splitting in the copper halides is significantly different compared to sp^3-hybridized materials [2]. In consequence, the electronic band structure of the copper halides in the zincblende phase has attracted much attention and has been investigated both experimentally and theoretically in many earlier studies. These have been critically reviewed [3].

Since that time considerable progress has been made. The technique of angle-resolved photoelectron spectroscopy now makes it possible to map experimental energy bands in considerable detail [4–6]. Improved methods to calculate the electronic energy bands of the copper halides have also been developed [2, 7, 8]. Consequently, we have tried to improve our experimental knowledge of the copper halide band structures. New results for CuCl,

† On leave of absence from the Institute of Mathematics and Physics, Academy of Technology and Agriculture, Bydgoszcz, Poland.

0953-8984/93/233827+10$07.50

derived from angle-resolved spectroscopies of photoelectrons [9] and of secondary electrons [10] were published several years ago. In the present paper we report a new investigation of CuBr, based on angle-resolved photoemission from epitaxially grown CuBr(111). We compare our results to an available band structure calculation [7] and to other relevant experimental results: UV absorption spectra [11], UV reflection spectra [12], x-ray absorption data [13] and recent results from 'constant-initial-state' photoelectron spectroscopy [14].

2. Experimental details

Most of the measurements were performed using an ESCA 100 spectrometer from Vacuum Science Workshops Ltd. It consists of two ultra-high-vacuum chambers which are pumped separately to a base pressure of 1×10^{-10} mbar. They are separated by a gate valve and are used for sample preparation and electron angle and energy analysis.

The spectrometer is equipped with a LEED facility, excitation sources for XPS (Mg Kα, Al Kα), UPS (a self-built capillary discharge lamp to excite the Ne I, He I and He II emission) and the standard sample preparation apparatus. Angular distributions are measured by rotating the crystal through the manipulator axis, thereby keeping the angle between the incident photon beam and the electron take-off direction constant ($\simeq$45° for UPS results). In all angle-resolved photoemission experiments the angular resolution was set to 4° (acceptance cone of the lens) and the energy resolution as determined by the constant energy flux through the analyser was chosen to be 100 meV.

Additional experiments were performed using the monochromatized synchrotron radiation of the storage ring BESSY in Berlin. In that instance we used the TGM 2-beamline and a high resolution photoelectron spectrometer based on a modified Vacuum Generators ADES 400 analyser. For these experiments the angular resolution was about 2° and the total energy resolution (for photons and electrons) was set to 200 meV.

The CuBr(111) samples were prepared by epitaxial growth of CuBr on a Cu(111) bulk single crystal. The latter was treated before by the standard procedures of argon-ion bombardment and gentle annealing. The substrate cleanliness and surface quality were verified by LEED and detailed UPS investigations of the well known Cu(111) surface states [15, 16] around the $\bar{\Gamma}$ and the $\bar{M}$ points of the surface Brillouin zone.

During the evaporation of CuBr from powdered CuBr the Cu(111) substrate was held at room temperature. The evaporation rate (about 10 monolayers per hour) was controlled with a quartz thickness monitor. The deposited film thickness was also checked via XPS core-level intensities using electron mean free path from [17] and calculated XPS excitation cross section ratios [18].

The CuBr(111) samples studied in the present work were typically at least 10 monolayers thick with a sufficient degree of photoconductivity to avoid any charging. No UPS features related to substrate emission were detected. We have observed a LEED pattern at a primary electron energy of 66 eV, which shows nearly hexagonal symmetry. The spots were less sharp and superimposed to increased background intensity as compared to the brilliant LEED pattern of the clean copper substrate. The ratio of lattice constants

$$\frac{a_{\mathrm{CuBr}}}{a_{\mathrm{Cu}}} = 1.58$$

was reproduced to within 5% experimental error.

Samples kept at room temperature during photon irradiation show severe damage effects. A typical result is shown in figure 1, where a polycrystalline film of CuBr (about 15 Å thick) evaporated onto a clean Ag(100) surface was illuminated by intense synchrotron radiation monochromatized at $\hbar\omega$ = 20 eV. Figure 1 shows photoelectron distribution curves from a new sample (labelled 1), from the same surface after 3 minutes (dashed, labelled 2) and after about 27 minutes of additional exposure (labelled 3). Besides the general loss of intensity and the smearing out of structural features, a new emission peak develops at about 4 eV below the Fermi energy E_F (E_F is defined by the substrate photoemission) which indicates a dramatic change in the electronic-structure. To avoid such decomposition effects the samples were cooled to 120 K during all measurements. At this temperature no changes in the photoelectron spectra were observed after several hours of irradiation with He and Ne resonance line photons of our laboratory source.

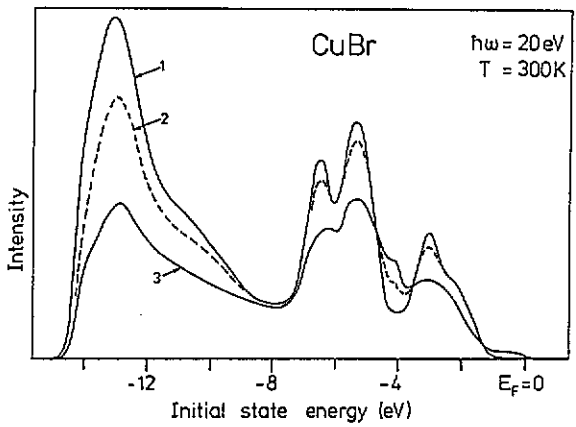

Figure 1. Photoemission spectra demonstrating photon-induced damage of a 15 Å thick CuBr film evaporated onto a clean Ag(100) crystal. Synchrotron radiation from BESSY was used for excitation at a photon energy of $\hbar\omega$ = 20 eV. Data refer to new sample (trace 1), sample after about 3 minutes of irradiation (dashed, trace 2) and after 27 minutes (trace 3). All data were taken while substrate was at room temperature.

3. Results

Two typical angle-resolved spectra taken at photon energies $\hbar\omega$ = 21.2 eV and $\hbar\omega$ = 40.8 eV in normal emission from a CuBr(111) film, held at 120 K are shown in figure 2. From earlier investigations of polycrystalline samples [3, 19] and from theoretical considerations [1, 3, 7] the structures labelled A–D may be assigned to their particular orbital-momentum character. The upper two features (A, B) overlap each other and the lower two (C, D) overlap each other. There is a gap between the upper pair and the lower pair. The upper bands (A, B) originate mainly from the 3d states of Cu, and the lower bands (C, D) from 4p states of bromine. In fact, peak B (originating from a state of Γ_{12} point group symmetry, in the non-relativistic notation [3] cannot hybridize with Br 4p orbitals and is essentially a pure d-like band. This fact is reflected by its very small dispersion as shown further below. Peak A (originating from a Γ_{15} state) contains some 4p admixture. In contrast, both peaks

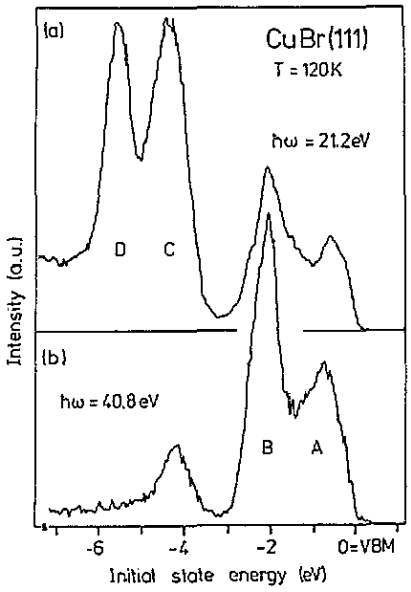

Figure 2. Normal emission photoelectron distribution curves taken from CuBr(111) at photon energies of $\hbar\omega$ = 21.2 eV (top) and $\hbar\omega$ = 40.8 eV (bottom). Data taken while sample was at 120 K and shielded against visible light.

C and D possess only weak d character: while peak D is almost purely of 4p origin, peak C contains some Cu 3d character.

Figure 2 also indicates the statistical quality of our data and shows our calibration of the valence band maximum (VBM). This calibration is chosen to be in agreement with all earlier data taken from polycrystalline samples and places the almost dispersionless peak B at (2.05 ± 0.10) eV below the VBM.

We have collected many angle-dependence spectra, at several photon energies. A typical result at $\hbar\omega$ = 40.8 eV is shown in figure 3. It indicates almost no dispersion of the peak at 2.05 eV below the VBM, however a strong dependence on the emission angle θ of the feature observed between the VBM and about 1.4 eV below the VBM. Our results generally originate from direct transitions occurring at many points in k-space. To localize these transitions in k-space and, in particular, to identify those data which correspond to the vicinity of the Γ–L direction, we make the usual assumption that the dominant final states of the photoemission process are those that can be best approximated by a free-electron-like band [4–6]

$$E_f(k) = \hbar\omega + E_i(k) = \left(\frac{\hbar^2}{2m}\right)k^2 + V_0. \tag{1}$$

In our terminology, energy conservation is given by $E_f - E_i = \hbar\omega$, and therefore we define the final state energy $E_f > 0$ and the initial state energy $E_i \leqslant 0$, where $E_i = 0$ coincides with the valence band maximum. In the extended zone scheme, conservation of electron momentum k is formulated as follows:

$$k_f = k_i + G(h, k, l)$$

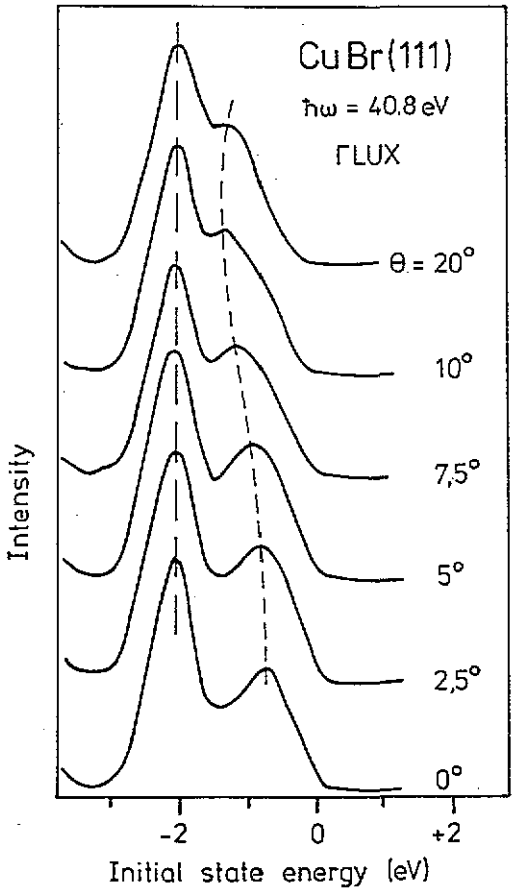

Figure 3. Angle-resolved photoelectron distribution curves taken from CuBr(111) at different emission angles Θ along the ΓLUX plane of the bulk Brillouin zone. Photon energy was $\hbar\omega$ = 40.8 eV.

where $G(h, k, l)$ is a reciprocal bulk lattice vector. During the transmission of the excited electron through the surface into the vacuum, only the component $k_\parallel$ parallel to the surface is conserved [20]. In contrast, $k_\perp = k - k_\parallel$ is changed by momentum transfer to the lattice, in order to ensure energy conservation during refraction, and therefore $k_\perp$ cannot be determined from the kinematics of only one electron distribution curve. Thus the usual approach to estimate $k_\perp$ is as follows: taking

$$k_\parallel = \sin\Theta[(2m/\hbar^2)E_{\text{kin}}]^{1/2}$$

from the experiment (where Θ is the electron take-off angle with respect to the surface normal, E_{kin} is the kinetic energy of the observed electron and m its rest mass) and making a reasonable assumption for V_0 (the average potential as seen by the electron within the bulk lattice) the component $k_\perp$ can be calculated from (1) with $G(h, k, l) = G(2, 2, 2)$.

The peak dispersion shown in figure 3 can be explained best with k-points, which are distributed over the ΓLUX emission plane of the bulk Brillouin zone of CuBr. The 'best' V_0 is determined by trial and error within the approximation of (1). We decided upon

$V_0 = -15$ eV which fits the He II off-normal data as well as the normal emission data measured at other photon energies (Ar I, Ne I, He I), using $a = 5.69$ Å for the lattice constant and $\Phi = 7.1$ eV [19] as the work function referred to the VBM. This particular choice appears reasonable since it is in fair agreement with the position of the Br(3s)-like band, which has been observed at $E_i = -15.4$ eV [19] and which is located close to the bottom of the inner potential. Note that the precise value of V_0 is not very critical, since (1) is only used to estimate

$$k_\perp = \sqrt{\left(\frac{2m}{\hbar^2}\right)(E_i + \hbar\omega - V_0) - k_\parallel^2}$$

while the initial state energy E_i and the component $k_\parallel$ of k are determined independently of the experimental data without any assumptions. Our choice of V_0 positions the series of spectra reproduced in figure 3 close to the Γ(2,2,2)L(3/2, 3/2, 5/2)Γ(1,1,3) line (in the extended reciprocal lattice scheme) within the ΓLUX plane. In fact, the remaining distance to the critical point Γ and L is not larger than the uncertainty of the k-vector caused by the life time broadening of the final electron state, as estimated from the observed peak widths. The then expected periodicity along Γ(2,2,2)L(3/2, 3/2, 5/2)Γ(1,1,3)L(1/2, 1/2, 7/2) is indeed observed in all our data (not reproduced), which were obtained up to $\Theta = 50°$ in $\Delta\Theta = 2.5°$ increments. While Γ is nearly reached at $\Theta = 0°$ and $\Theta = 39.6°$, the L point is touched near $\Theta = 18.8°$ (compare figure 3) and approached again at $\Theta > 45°$. This allocation is also fully consistent with the respective $k_\parallel$-vectors, which can be derived from the kinematics without any further assumptions. Thus our choice of V_0 at least guarantees an almost complete inner consistency of our results. We are thus able to derive an 'approximate' band structure along Γ–L from experimental data which correspond to direct transitions occuring very near to the Γ–L-symmetry line. In fact we estimate the errors in $k_\perp$ to be below 5% of the characteristic dimensions of the bulk Brillouin zone. Considering the weak dispersion of the bulk bands with $k_\perp$ in all k-space directions where calculations are available [7, 19] (compare also figure 4) we are confident that our results reflect the bulk band structure along Γ–L within the given error margins.

A summary of all our results plotted along the Γ–L bulk Brillouin zone direction is shown in figure 4. Also reproduced in this figure are the results of the calculation performed by Overhof [7] along the same k-space line.

4. Discussion

Comparison between the experimental and theoretical energy bands compiled in figure 4 indicates a generally good qualitative overall agreement. Closer inspection reveals quantitative differences. In particular the width of the upper bands is observed to be about 2.1 eV, while the calculation predicts 1.3 eV. However, the lower bands with a calculated width of 1.4 eV agree reasonably well with the observed width of 1.25 eV. The gap between upper and lower bands is observed to be 2.1 eV, not very different from the calculated 2.3 eV. Also the initial state energy of the uppermost flat band of the lower ones has been calculated to be $E_i = -3.7$ eV, reasonably close to -4.2 eV as observed experimentally. Thus, apart from the width of the upper bands, calculation and experiment are in fair agreement.

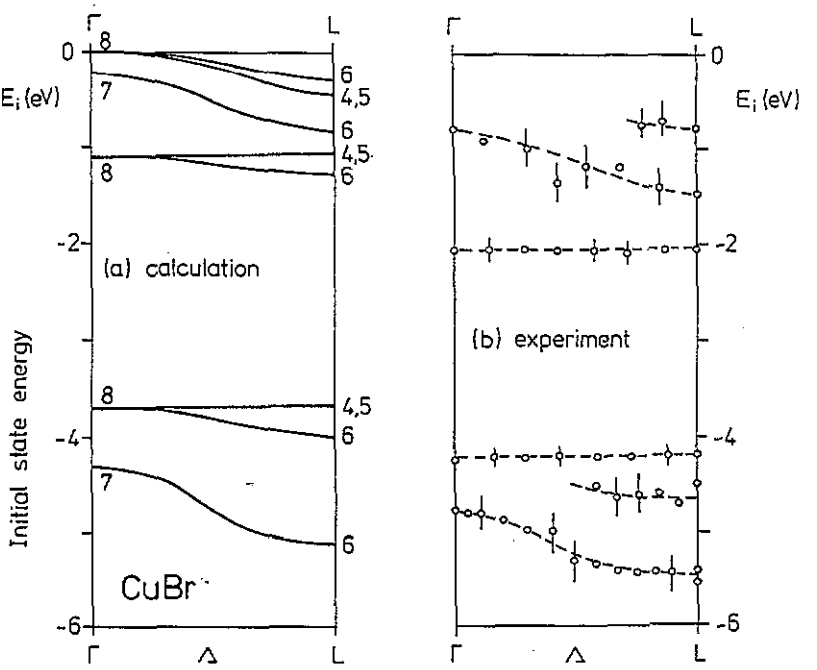

Figure 4. Band structure of CuBr along the Γ–L direction of the bulk Brillouin zone: (*a*) calculated by Overhof [7], (*b*) experimental results of present work. The error in $k_\perp$ is about 10% of the distance Γ–L for all data points.

Table 1. Critical point energies of CuBr valence bands along the Γ–L direction in the bulk Brillouin zone. Errors are given in brackets in units of 0.1 eV.

Initial states E_i (eV)	Assignment	*l*-character
−15.4(3)†	Γ_6;L_6	s
− 5.6(3)	L_6	p
− 4.8(3)	Γ_7	p
− 4.7(3)	L_6	p + (d)
− 4.2(2)	Γ_8;$L_{4,5}$	p + (d)
− 2.05(1)	Γ_8;L_6;$L_{4,5}$	d
− 1.4(3)	L_6	d + (p)
− 0.8(3)	$\Gamma_{7,8}$;L_6;$L_{4,5}$	d + (p)

† Data from [19].

The band structure calculation of Overhof [7] is based on the relativistic Korringa–Kohn–Rostoker (KKR) method, using a potential of the muffin-tin form. His data as reproduced in figure 4 are calculated with a potential constructed from SCF atomic potentials, overlapped and cast into a muffin-tin form. Overhof also performed a calculation using ionic potentials. The results, not reproduced here, show very similar overall behaviour, but of course quantitative differences. Now the width of the upper bands is increased to about 1.9 eV, in almost perfect agreement with the experimental value of (2.05±0.10) eV. However, the width of the lower bands is reduced by a factor of about two, making the

Table 2. Critical point energies of CuBr conduction states as obtained from 'constant-initial-state' spectroscopy (CIS) and from secondary electron emission (SEE) spectra. Errors (in brackets) are given in units of 0.1 eV .

Final state energies E_f (eV)			
CIS	SEE†	SEE‡	Predominant *l*-character
7.7(5)	7.5	7.4(2)	p
8.9(2)	8.8	8.9(3)	s, d
10.2(2)	—	—	s, d
12.0(5)	—	—	
14.1(2)	—	—	p, f
15.2(2)	—	—	s, d
17.2(2)	—	—	p, f

† [21].
‡ This work.

agreement with the photoemission data much worse, and the gap between the upper and the lower group of bands is reduced drastically from 2.3 eV to about 1.1 eV. We conclude that our data are best described by the calculation based on atomic potentials.

One might speculate whether the discrepancy in the width of the uppermost bands could be due to a relaxation (photoemission final state) effect, since only the bands with predominant d-orbital character are affected. We have no experimental means to answer this question. Another explanation should also be considered seriously: if our calibration of $E_i = 0$, i.e. the definition of the valence band minimum, was wrong by about 0.6–0.7 eV, nearly perfect agreement with the calculated bands could be reached. Indeed, group theoretical arguments lead to a direct gap at Γ in the zincblende lattice of CuBr. The spin–orbit splitting at Γ, i.e. $E_i(\Gamma_8)-E_i(\Gamma_7)$ at the VBM, was observed to be about 0.15 eV [1]. If we add this energy to the uppermost experimental band observed at $E_i = -0.8$ eV, we end up with an 'adjusted' VBM at $E_i = -0.65$ eV in figure 4(*b*). The obtained bandwidth of 1.5 eV compares well to the calculated 1.3 eV. However, we have no reason to think that our calibration of $E_i = 0$ could be wrong by more than half of an electronvolt.

The fair agreement between experimental and theoretical energy bands encouraged us to assign symmetry labels according to figure 4(*a*) to the Γ- and L-point energies as observed in figure 4(*b*). All results concerning initial valence state energies are collected in table 1. Information about final stage energies involved in the photoemission from CuBr results from the analysis of secondary electron emission (SEE) structures in the electron energy distribution curves and, in particular, from 'constant-initial-state' (CIS) spectra taken earlier by us [14] from polycrystalline films of CuBr. The energies of significant peaks in CIS-results as well as structures due to secondary electrons (observed in the present work and also earlier by Lin *et al* [21] are summarized in table 2. Note that all energies given in this table for $E_f > 0$ and in table 1 for $E_i \leqslant 0$ refer to the same calibration of the VBM, which is used also in figure 4(*b*).

Next we demonstrate that our results are consistent with optical data. The first column of table 3 summarizes prominent transitions observed in ultraviolet reflection [12], ultraviolet absorption [11] and soft x-ray absorption [13] spectra. The second and third columns give our interpretation in terms of interband transitions between the states listed in tables 1 and 2, respectively.

Of course, a unique fit of the optical data is not possible in general. Nevertheless table 3 indicates that our results are consistent within typically ± 0.1 eV with all other available

Table 3. Interpretation of optical transitions listed in column 1, in terms of interband transitions between states listed in tables 1 and 2, respectively.

Optical transition method	$\hbar\omega$ (eV)	$\hbar\omega$	Interpretation $E_i \rightarrow E_f$
a	9.0	8.9	L_6 (−1.4 eV) → + 7.5 eV
b	9.1		L_6 (−2.1 eV) →
b	11.0	11.0	L_6 (−2.1 eV) → + 8.9 eV
c	≈ 12.1	≈ 12.1	$L_{4,5}$ (−4.2 eV), Γ_6 (−4.7 eV), Γ_7(−4.8 eV) → + 7.5 eV
b	13.4		$L_{4,5}$ (−4.2 eV), Γ_6 (−4.7 eV), Γ_7 (−4.8 eV) → + 8.9 eV
		≈ 13.5	
a	13.6		
b	16.1	16.2	Γ_8 (−4.2 eV) → + 12.0 eV; Γ_8 (2.1 eV) → + 14.1 eV
a	≈ 16.5	16.6	L_6 (−1.4 eV) → + 15.2 eV
b	17.1	≈ 17.0	VBM → + 17.2 eV, Γ_7 (−4.8 eV) → + 12 eV
c	≈ 17.5	≈ 17.5	VBM → 17.2 eV; L_6 (−5.6 eV) → + 12 eV
b	19.8	19.9	L_6 (−4.7 eV) → + 15.2
b	22.1	22.0	Γ_7 (−4.8 eV) → 17.2

(a) UV absorption [11].
(b) UV reflection [12].
(c) Soft x-ray absorption [13].

data. Also all interpretations listed in table 3 satisfy the common selection rule for optical dipole transitions.

In conclusion we have obtained new band structure data for CuBr. All available optical results of other authors are fully consistent with our results. We hope our work stimulates further theoretical and experimental work, in particular to obtain a better description of the conduction states.

Acknowledgments

Our work has been supported by the Bundesministerium für Forschung und Technologie and by the Deutsche Forschungsgemeinschaft. J Skonieczny thanks Dr Wilhelm Heinrich and Else Heraeus Stiftung for the grant that made his stay at Kassel possible.

References

[1] Cardona M 1963 *Phys. Rev.* **129** 69
[2] Blacha A, Cardona M, Christensen N E, Ves S and Overhof H 1982 *Solid State Commun.* **43** 183
[3] Goldmann A 1977 *Phys. Status Solidi* b **81** 9
[4] Plummer E W and Eberhardt W 1982 *Adv. Chem. Phys.* **49** 533
[5] Himpsel F J 1983 *Adv. Phys.* **32** 1
[6] Courths R and Hüfner S 1984 *Phys. Rep.* **112** 53
[7] Overhof H 1980 *Phys. Status Solidi* b **97** 267
[8] Ves S, Glötzel D, Cardona M and Overhof H 1981 *Phys. Rev.* B **24** 3073
[9] Westphal D and Goldmann A 1982 *J. Phys. C: Solid State Phys.* **15** 6661
[10] Goldmann A and Westphal D 1983 *J. Phys. C: Solid State Phys.* **16** 1335
[11] Ishii T, Sato S, Matsukawa T, Shaisako Y and Sagawa T 1972 *J. Phys. Soc. Japan* **32** 1440
[12] Gross J C, Lewonczuk S, Khan M A and Ringeissen J 1980 *Solid State Commun.* **36** 907
[13] Beeman W W, Forss J and Humphrey J N 1945 *Phys. Rev.* **67** 217

[14] Skonieczny J, Lodders F, Engelhard H, Goldmann A, Johnson R L and Ghijsen C 1991 *Z. Phys.* B **85** 211
[15] Heimann P, Hermanson J, Miosga H and Neddermeyer H 1979 *Phys. Rev.* B **20** 3059
[16] Westphal D and Goldmann A 1980 *Surf. Sci.* **95** L249
[17] Seah M P and Dench W A 1979 *Surf. Interface Anal.* **1** 2
[18] Scofield J H 1976 *J. Electron Spectrosc. Relat. Phenom.* **8** 129
[19] Goldmann A, Tejeda J, Shevchik N J and Cardona M 1974 *Phys. Rev.* B **10** 4388
[20] Mahan G D 1970 *Phys. Rev.* B **2** 4334
[21] Lin S F, Spicer W E and Bauer R S 1976 *Phys. Rev.* B **14** 4551